ELSEVIER

Contents lists available at ScienceDirect

Dyes and Pigments

journal homepage: www.elsevier.com/locate/dyepig





Zinc(II) complexes of azadipyrromethene: Effect of nature and placement of solubilizing groups on structural, thermal, electrochemical and optical properties

Jayvic C. Jimenez^a, Quynh Tran^a, Madison H. Pugh^a, Christina D. Brancel^a, Arnold L. Rheingold^b, Geneviève Sauvé^{a,*}

ARTICLE INFO

Keywords: Non-planar chromophores Non-fullerene acceptors Side-chain engineering

ABSTRACT

Zinc(II) complexes of azadipyrromethenes are non-planar chromophores with strong absorption in the visible to NIR and are promising n-type materials for organic solar cells. To increase solubility and tune their properties, we incorporated hexyl or hexyloxy solubilizing groups either on the distal or proximal phenyls of bis[2,6-diphenylethynyl-1,3,7,9-tetraphenyl azadipyrromethene] zinc(II) (Zn(WS3)₂). Crystal structures confirm the typical distorted tetrahedral geometry for these types of complexes and show that the solubilizing groups on the distal phenyls extend away from the conjugated core whereas groups on proximal phenyls interact with the other ligand. Differential scanning calorimetry measurement indicated that crystals of distal-substituted complexes have two endothermic peaks: solubilizing groups 'melting' and complex melting, whereas the proximalsubstituted complexes show one exothermic crystallization peak and one endothermic melting peak. Electrochemical and optical properties varied as expected for ADP-based complexes: the presence of electron rich groups at the proximal substitutions resulted in lower oxidation potentials, higher HOMO levels, red-shifted absorption and lower optical gap than distal substitutions, and the effect was greater for hexyloxy than hexyl. Upon thermal annealing, films of the hexyloxy-substituted complexes strongly aggregated and showed crystal features under a polarized microscope, indicating that hexyloxy groups drive ordered self-assembly, especially when placed on distal phenyls. The ability to guide solid-state self-assembly of these non-planar chromophores using solubilizing groups have the potential to improve their charge carrier mobility and performance in opto-electronic applications such as organic solar cells, and photodetectors.

1. Introduction

Azadipyrromethenes are a class of chromophores with strong absorption in the visible to near infrared absorption, tunable properties through substitution and chelation, and high electron affinity [1–3]. They are typically coordinated with boron such as BF_2^+ or intramolecularly with B–O. and have been investigated for applications including bioimaging, photodynamic therapy, near-infrared sensing and organic photovoltaics (OPVs) [4–9]. The Sauvé group have demonstrated that homoleptic zinc(II) complexes of azadipyrromethene are promising candidates as electron acceptor for OPVs [10]. Bis(2,6-diphenyle-thynyl-1,3,7,9-tetraphenylazadipyrromethene) ($Zn(WS3)_2$, Fig. 1) showed a power conversion efficiency (PCE) of up to 4% when paired

with poly(3-hexylthiophene) (P3HT) as the electron donor. It has a strong absorption from 600 to 800 nm, which complements that of P3HT. The phenylethynyl groups at the pyrrolic positions are critical to increase electron affinity, increase the conjugation system and obtain a favorable blend morphology when blended with P3HT [11]. The complex's non-planar geometry reduces the tendency for the conjugated ADP ligands to self-aggregate, thus remaining amorphous in films. We have been improving the complexes' opto-electronic properties through structure-property studies [12]. We found that the electron mobility and performance can be improved with fluorination [13]. We also explored changing the phenyl in the phenylethynyl groups with larger aryl groups such as naphthyl and phenanthrenyl. However, these larger groups significantly reduced the complex solubility in organic solvents. It was

E-mail address: genevieve.sauve@case.edu (G. Sauvé).

^a Department of Chemistry, Case Western Reserve University, 10900 Euclid Avenue, Cleveland, OH, 44106-7078, United States

b Department of Chemistry and Biochemistry, University of California, San Diego, La Jolla, CA, 92093, United States

^{*} Corresponding author.

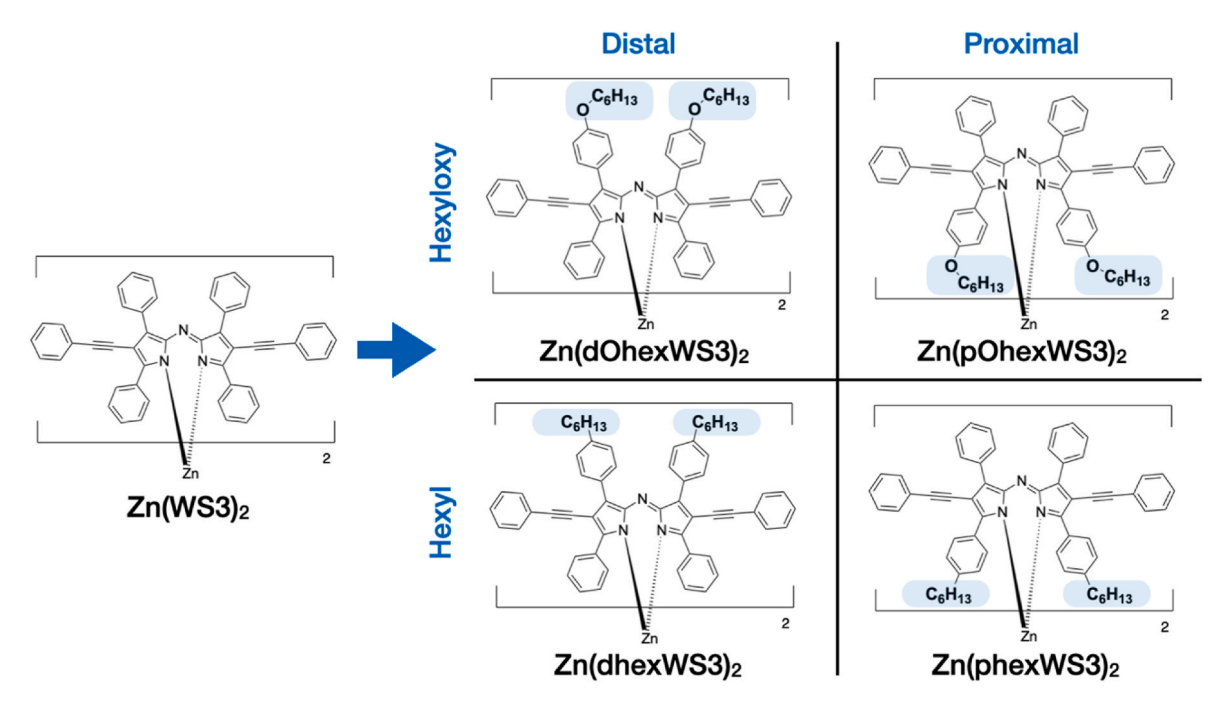


Fig. 1. Chemical structure on Zn(WS3)2 and the four complexes with either hexyl or hexyloxy placed on the distal- or proximal-phenyls.

thus necessary to add solubilizing groups. We showed that the complex with 1-naphthylethynyl pyrrolic groups and hexyls on the proximal phenyls had the best performance in OPVs with a PCE of 5.5% when blended with P3HT [14,15]. Both the larger 1-naphthyl group and the hexyl solubilizing groups contributed to increase the tendency for these complexes to crystallize.

It is well known in the conjugated molecule and polymer field that solubilizing groups affect self-assembly and morphology in films by disfavoring random aggregation and encouraging the formation of favorable crystal packing [16–18]. The choice of alkoxy group instead of hexyl groups has also been shown to affect molecular packing and improve photovoltaic performance [19–21]. In addition, the electron donating nature of these groups also tunes their optical and electrochemical properties by increasing the HOMO energy levels without greatly affecting the LUMO energy level [22,23]. We note that most studies of the effect of solubilizing groups on properties use planar conjugated systems; the effect of solubilizing groups on properties of non-planar conjugated molecules is under-investigated.

The zinc(II) complexes of ADP are non-planar conjugated molecules and thus a good place to start investigations. In particular, we do not understand how the nature and placement of solubilizing groups will affect the complexes' properties. To fill this gap, we designed, synthesized and studied a series based on the non-planar Zn(WS3)₂ complex where either hexyl or hexyloxy groups were installed on either the distal or proximal phenyls, as depicted in Fig. 1. Since Zn(WS3)₂ was already soluble in a variety of organic solvents, the solubility of the new complexes was not measured. The structural, thermal, electrochemical and optical properties are reported.

2. Materials and methods

2.1. Materials

Solvents were freshly distilled and stored with 3 Å molecular sieves prior to use. Chemicals were purchased from Sigma-Aldrich, Fisher or Acros organics and were used as received.

2.2. Synthesis

The following compounds were synthesized according to the literature: 4-Hexylbenzaldehyde (1b) [9], 4-hexylbenzaldehyde (1c) [9], 4-hexylacetophenone (2b) [14], 4-hexyloxychalcone (3a) [9], dOhexADP (4a) [9], dOhexWS3 (5a) [9], and Zn(phexWS3)₂ (6d) [14].

(2c) 4'-hexyloxyacetophenone. 4'-hydroxyacetophenone (10.00 g, 73.45 mmol), 1-bromohexane (13.34 g, 80.79 mmol) and potassium carbonate (15.23 g, 110.2 mmol) was added into a 200 mL Erlenmeyer flask with 100 mL of DMF. The solution was stirred for 16 h under reflux then cooled to RT. The solution was stirred with 100 mL of DI-water then extracted with 5 x 25 mL aliquots of ethyl acetate. The top layer was collected then washed with 3 x 20 mL aliquots of DI-water, twice with brine, then dried with magnesium sulfate. The solution was evaporated via rotary evaporator then distilled using short-path distillation (bp: 131 °C, 0.07 Torr) as a clear, colorless oil. (10.14 g, 46.03 mmol, Yield: 62.66%). ¹H NMR (500 MHz, chloroform-d) δ 7.95–7.88 (m, 2H), 6.96–6.86 (m, 2H), 4.01 (t, J = 6.6 Hz, 2H), 2.54 (s, 3H), 1.79 (p, J = 6.8 Hz, 2H), 1.46 (q, J = 7.4 Hz, 2H), 1.34 (m, J = 3.3 Hz, 4H), 0.90 (t, J = 7.0 Hz, 3H). ¹³C NMR (126 MHz, CDCl₃) δ 196.92, 163.25, 130.69, 130.20, 114.24, 77.16, 68.38, 31.66, 29.18, 26.45, 25.77, 22.71, 14.14.

(3b) 4-hexylchalcone. See 4'-hexyloxychalcone (3c) for synthesis, using 4-hexylbenzaldehyde (3.00 g, 15.8 mol), acetophenone (1.89 g, 15.8 mol), and NaOH (1.89 g, 47.3 mol). The crude product was a fine off-white solid that was recrystallized in MeOH (2.56 g, 8.75 mol, yield: 55.5%). $^1\mathrm{H}$ NMR (500 MHz, chloroform-d) δ 8.09–7.93 (m, 2H), 7.80 (d, J=15.7 Hz, 1H), 7.57 (dd, J=7.5, 5.4 Hz, 3H), 7.54–7.46 (m, 3H), 7.23 (d, J=7.9 Hz, 2H), 2.64 (t, J=7.8 Hz, 2H), 1.63 (p, J=7.6 Hz, 2H), 1.43–1.12 (m, 6H), 0.94–0.83 (m, 3H). $^{13}\mathrm{C}$ NMR (126 MHz, CDCl₃) δ 190.86, 146.33, 145.18, 138.53, 132.81, 132.50, 129.21, 128.74, 128.66, 128.62, 121.28, 77.41, 77.16, 76.91, 36.10, 31.84, 31.37, 29.11, 22.74, 14.24.

(3c) 4'-hexyloxychalcone. 4'-hexyloxyacetophenone (2.50 g, 11.4 mmol), benzaldehyde (1.20 g, 11.4 mmol) and NaOH (1.36 g, 34.0 mmol) were added into a 200 mL Erlenmeyer flask with 100 mL of 80% MeOH in water. The mixture was stirred at RT for 16 h then filtered. The solids were recrystallized in MeOH then filtered. The solids were dried under vacuum into an off-white crystalline solid. (2.97 g, 9.63 mmol, Yield: 84.9%). 1 H NMR (500 MHz, chloroform-d) δ 8.03 (d, J = 8.7 Hz,

2H), 7.80 (d, J=15.6 Hz, 1H), 7.64 (dd, J=7.1, 2.6 Hz, 2H), 7.55 (d, J=15.7 Hz, 1H), 7.41 (h, J=3.4 Hz, 3H), 6.97 (d, J=8.7 Hz, 2H), 4.03 (t, J=6.6 Hz, 2H), 1.81 (p, J=6.8 Hz, 2H), 1.47 (dd, J=10.5, 4.6 Hz, 2H), 1.35 (dp, J=7.5, 4.6, 3.9 Hz, 4H), 0.91 (t, J=6.9 Hz, 3H). 13 C NMR (126 MHz, CDCl₃) δ 188.83, 163.21, 143.98, 135.21, 130.92, 130.41, 129.02, 128.46, 122.01, 114.41, 68.40, 31.66, 29.19, 25.78, 22.70, 14.15.

General Method for ADP Synthesis. Chalcones were added into a 200 mL round-bottom flask with 5 equivalents of nitromethane and 10 equivalents of diethylamine with 150 mL of MeOH. The mixture was stirred for 16 h under reflux. The solution was cooled to 0 $^{\circ}$ C via ice bath, neutralized with 1 M HCl until pH \sim 1, and then filtered. The filtered solids were placed in a 100 mL round-bottom flask along with 35 equivalents of ammonium acetate and 150 mL of 1-BuOH, as a suspension. The suspension was stirred under reflux for 16 h which eventually dissolved all of the solids, resulting in a dark colored solution. Approximately half of the solvent was removed via rotary evaporation, then filtered and washed with cold methanol, dried, then washed with hexanes. The resulting solid is a metallic colored solid that was used as is in the next step.

(4b) dhexADP. 4-hexylchalcone (2.00 g, 6.84 mmol), nitromethane (2.09 g, 34.2 mmol) and diethylamine (5.00 g, 68.4 mmol) were added in a 200 mL round-bottom flask. The filtered solids were added into a 100 mL flask with ammonium acetate (18.45 g, 239.4 mmol) and 75 mL of 1-BuOH. The collected solid was dried under vacuum overnight resulting in a metallic yellow/blue solid (304 mg, 0.492 mmol, Yield: 14.4%). MALDI-TOF: 617.302 m/z. Calc'd: 617.38 m/z. 1 H NMR (500 MHz, chloroform-d) δ 12.73 (s, 1H), 8.02 (d, J = 7.9 Hz, 4H), 7.97 (dd, J = 7.1, 1.8 Hz, 4H), 7.55 (t, J = 7.5 Hz, 4H), 7.48 (t, J = 7.2 Hz, 2H), 7.28 (d, J = 5.7 Hz, 4H), 7.19 (s, 2H), 2.71 (t, J = 7.7 Hz, 4H), 1.71 (p, J = 7.4 Hz, 4H), 1.43 (p, J = 6.3 Hz, 4H), 1.41–1.33 (m, 8H), 0.94 (t, J = 7.1 Hz, 6H).

(4c) pOhexADP. 4'-hexyloxychalcone (6.00 g, 19.5 mmol), nitromethane (3.56 g, 29.2 mmol), diethylamine (4.27 g, 58.4 mmol) were added into the flask. Next ammonium acetate (54.48 g, 0.681 mol) were added with 100 mL of 1-BuOH. The resulting solid was a metallic yellow color (3.26 g, 5.02 mmol, 51.6% yield). MALDI-TOF: 617.302 m/z. Calc'd: 617.38 m/z. 1 H NMR (500 MHz, chloroform-d) δ 12.70 (s, 1H), 8.06 (d, J=7.6 Hz, 4H), 7.87 (d, J=8.3 Hz, 4H), 7.38 (dt, J=37.7,7.4 Hz, 6H), 7.12 (s, 2H), 7.03 (d, J=8.3 Hz, 4H), 4.05 (t, J=6.6 Hz, 4H), 1.84 (p, J=6.9 Hz, 4H), 1.51 (p, J=7.4 Hz, 4H), 1.45–1.25 (m, 8H), 0.94 (t, J=6.5 Hz, 6H). 13 C NMR (126 MHz, CDCl₃) δ 161.03, 154.38, 149.49, 142.16, 134.09, 129.16, 128.34, 128.23, 127.90, 124.93, 115.29, 114.37, 77.41, 77.16, 76.91, 68.43, 31.75, 29.35, 25.88, 22.78, 14.21. MALDI-TOF: 650.433 m/z (Calc'd: 649.37 m/z).

General synthesis for diiodination. Compound 4 was weighed out into a 250 mL round-bottom flask. 200 mL of chloroform was added and then degassed with N_2 for 15 min. N-iodosuccinimide (NIS, 2.3 equiv.) and ten drops of acetic acid were added, and the solution was stirred overnight and kept away from light. The solution was evaporated and then resuspended in methanol. The compound was filtered then washed with ethyl acetate until the filtrate is colorless. The solids were dried overnight and used directly in the next step. For the synthesis of pOhexADPI2, a slightly different synthesis was employed. Half the amount of NIS was added initially. After reacting overnight under foil at room temperature, the second half of NIS was added and stirred overnight away from light.

General synthesis for Stille coupling of phenylethynyl groups. From the previous step, solids were placed into a 250 mL Schlenk flask and evacuated and refilled with N_2 three times. The flask was transferred into a glove box to which $Pd(PPh_3)_4$ (0.10 equiv.) was added. The flask was then transferred out of the glove box and placed under a N_2 atmosphere. 75 mL of dry xylenes were added via cannula and the solution was stirred. Tributyl(phenylethynyl)tin (2.3 equiv) was added dropwise via syringe. The solution was then heated to 135 °C and was left to stir overnight. The solution was evaporated via rotary evaporator, washed

with ethyl acetate, filtered then rinsed with hot ethyl acetate until the filtrate was colorless. The solids were dried under vacuum overnight. The solids were used directly in the next step. The solids were poorly soluble in deuterated solvents and no NMR spectra were obtained.

(5b) dhexWS3. Compound 4b (504 mg, 0.809 mmol) and N-iodo-succinimide (422 mg, 1.86 mmol) were used. The resulting iodinated 4b is a purple, shiny solid. (Yield: 576 mg, 0.662 mmol, 81.20%). $^1\mathrm{H}$ NMR (500 MHz, chloroform-d, Fig. S13) δ 12.21 (s, 1H), 7.99–7.94 (m, 4H), 7.64 (d, J=7.7 Hz, 4H), 7.56–7.45 (m, 6H), 7.18 (d, J=7.8 Hz, 4H), 2.68–2.61 (m, 4H), 1.72–1.62 (m, 4H), 1.47–1.29 (m, 12H), 0.95–0.89 (m, 6H). The solids were directly used for the next step. Solids from the previous step (0.830 g, 0.609 mmol), Pd(PPh_3)_4 (70 mg, 0.061 mmol and tributyl(phenylethynyl)tin (548 mg, 1.40 mmol) were added. The resulting product was a shiny purple solid and was not fully purified due to very limited solubility in organic solvents. (456 mg, 0.557 mmol, 91.5% yield). MALDI-TOF: 817.467 m/z. (Calc'd: 817.64 m/z).

(5c) pOhexWS3: Compound 4c (500 mg, 0.770 mmol) and N-iodosuccinimide (196 mg (1st); 198 mg (2nd), 1.75 mmol total) were used. Half of the N-iodosuccinimide was added on the first day and the solution was left stirring overnight under foil. Half the N-iodosuccinimide was added on the second day and the solution was left stirring overnight under foil again. The resulting iodinated 4c was a purple/blue, shiny solid. (Yield: 560 mg, 0.621 mmol, 80.7%). ¹H NMR (500 MHz, chloroform-d, Fig. S12) δ 12.20 (s, 1H), δ 7.96 (d, J = 8.4 Hz, 4H), 7.73–7.66 (m, 4H), 7.40-7.31 (m, 6H), 7.04-6.99 (m, 4H), 4.05 (t, J = 6.5 Hz, 4H),1.89-1.79 (m, 4H), 1.64-1.45 (m, 8H), 1.37 (dt, J = 7.3, 4.1 Hz, 8H), 0.98-0.90 (m, 6H). The solids were directly used for the next step. Solids from previous step (300 mg, 0.333 mmol), Pd(PPh₃)₄ (38.45 mg, 0.033 mmol), and tributyl(phenylethynyl)tin (306 mg, 0.782 mmol) were added. The resulting product was a shiny purple/blue solid and was not fully purified due to very limited solubility in organic solvents. (Yield: 298, 0.350 mmol, 105.0% (the isolated yield is larger than 100% due to impurities). MALDI-TOF: 849.583 m/z. (Calc'd: 849.43 m/z).

General Procedure for Zn(II) chelation. Compound 5 was placed in a 50 mL Schlenk flask with a stir bar. The flask was evacuated and refilled with N_2 three times. Then 20 mL of THF was added via cannula transfer and stirred for 5 min, then NaH (3.5 equiv) or lithium diisopropylamide (2.0 M in hexanes, 5 equiv) was added and left to stir for 2 h. A solution of 0.7 M ZnCl $_2$ (5 equiv) in diethyl ether was added via syringe dropwise followed by 5 mL of methanol then stirred for 24 h. The solution was passed through a plug of celite then purified via column chromatography. The purified complexes were then recrystallized from vapor diffusion from either DCM or THF with methanol.

(6a) Zn(dOhexWS3)₂. Compound 5a (325 mg, 0.370 mmol), NaH (30 mg, 1.3 mol), and ZnCl₂ (2.64 mL, 1.85 mmol) were used. The final product was purified by column chromatography using a silica gel column and 3:1 hexanes:DCM. The solution was evaporated and afforded metallic-red solids. The solids were recrystallized with THF:MeOH solvent diffusion as a metallic-red needle-like crystals. (Yield: 156 mg, 0.857 mmol, 46.3%) $^1{\rm H}$ NMR (500 MHz, chloroform-*d*) δ 8.03–7.92 (m, 8H), 7.83–7.68 (m, 8H), 7.40–7.15 (m, 32H), 7.07–6.93 (m, 8H), 4.11 (t, J=6.6 Hz, 8H), 1.90 (p, J=6.9 Hz, 8H), 1.57 (p, J=6.6 Hz, 8H), 1.48–1.34 (m, 16H), 0.97 (t, J=6.8 Hz, 12H). MALDI-TOF: 1761.151 m/z (Calc'd: 1760.77 m/z). Elemental Analysis: C 81.49, H 6.49, N 4.51; calc'd: C 81.73, H 6.17, N 4.77.

(6b) Zn(dhexWS3)₂. Compound 5b (150 mg, 0.183 mmol), NaH (15.4 mg, 0.642 mmol) and 0.7 M ZnCl₂ (1.31 mL, 0.917 mmol) were used. The product was purified by column chromatography using silica gel and 10:1 hexanes:EtOAc. The solution was evaporated and afforded metallic-red solids. The solids were recrystallized with DCM:MeOH solvent diffusion as metallic-red needle-like crystals (Yield: 70.0 mg, 0.412 mmol, 44.9%). ¹H NMR (500 MHz, chloroform-d) δ 7.94 (d, J = 7.9 Hz, 8H), 7.79–7.70 (m, 8H), 7.41–7.33 (m, 8H), 7.33–7.24 (m, 20H), 7.25–7.16 (m, 12H), 2.76 (t, J = 7.9 Hz, 8H), 1.79 (p, J = 7.6 Hz, 8H), 1.50 (p, J = 6.9 Hz, 8H), 1.47–1.38 (m, 16H), 0.96 (t, J = 7.0 Hz, 12H). ¹³C NMR (126 MHz, CDCl₃) δ 162.05, 147.00, 145.85, 143.37, 132.69,

Scheme 1. Synthesis of Zn(II) complexes: a) NaOH, in 80% MeOH stirred in RT for 24 h, b) diethylamine, nitromethane stirred in MeOH, reflux, c) ammonium acetate, 1-BuOH, reflux, d) N-iodosuccinimide and AcOH, in degassed CHCl₃ for 16 h, e) phenylethynyl tributyltin, Pd(PPh₃)₄ in xylenes 135 °C, f) NaH or LDA, ZnCl₂ in THF at 75 °C.

131.45, 131.21, 131.01, 130.24, 128.68, 128.63, 128.18, 124.38, 111.77, 96.88, 85.91, 77.16, 36.61, 32.33, 32.05, 29.78, 23.15, 14.60. MALDI-TOF: 1697.126 m/z (Calc'd: 1696.79 m/z). Elemental Analysis: C 84.38, H 6.32, N 4.97; calc'd: C 84.80, H 6.41, N 4.94.

(6c) Zn(pOhexWS3)2. Compound 5c (283 mg, 0.333 mmol), sodium hydride (23.50 mg, 0.979 mmol), and ZnCl₂ (1.66 mL, 1.66 mmol) were used. The product was purified by column chromatography using silica gel and 3:1 hexanes:DCM. The solution was evaporated and afforded metallic-red solids. The solids were recrystallized with THF:pentanes vapor diffusion as a metallic-red orthorhombic crystals. (Yield: 97.0 mg, 0.0550 mmol, 62.3%). ¹H NMR (500 MHz, chloroform-d) δ 8.04 (dd, J =6.6, 2.8 Hz, 8H), 7.74 (d, J = 8.5 Hz, 8H), 7.40 (ddd, J = 21.6, 6.3, 1.8 Hz, 20H), 7.30 (d, J = 7.6 Hz, 12H), 6.73 (d, J = 8.3 Hz, 8H), 3.54 (t, J =7.0 Hz, 8H), 1.56 (p, J = 6.8 Hz, 8H), 1.31 (p, J = 7.3 Hz, 8H), 1.28–1.15 (m, 16H), 0.91 (t, J = 7.1 Hz, 12H). ¹³C NMR (126 MHz, CDCl₃) δ 161.39, 160.97, 146.66, 144.88, 133.36, 131.18, 131.03, 129.97, 128.45, 127.96, 127.90, 127.64, 124.71, 124.14, 113.81, 111.73, 96.68, 85.93, 77.42, 77.16, 76.91, 68.30, 31.78, 29.19, 25.63, 22.80, 14.25. MALDI-TOF: 1761.114 m/z (Calc'd: 1760.77 m/z). Elemental Analysis: C 81.60, H 5.95, N 4.71; calc'd: C 81.73, H 6.17, N 4.77.

2.3. Measurements

Nuclear magnetic spectroscopy (NMR) measurements were obtained using a 500 MHz Bruker Ascend Advance III High Definition, using CDCl₃ as the reference solvent, obtained from Fisher. Matrix-assisted laser desorption/ionization time-of-flight (MALDI-TOF) mass spectra measurements were obtained on a Bruker Autoflex III MALDI-TOF mass spectrometer, using a solution of terthiophene (Sigma-Aldrich) as the

matrix in CHCl₃. Elemental analysis (C, H, and N) was performed by Robertson Microlit Laboratories (Ledgewood, NJ).

UV–Vis absorption spectra were obtained from a Cary 5000 UV–Vis–NIR spectrophotometer. Solutions were prepared from a 0.1 mg/mL stock solution with HPLC-grade CHCl $_3$. Samples were measured using a quartz cuvette with a 1 cm pathlength. To measure the absorption of the complexes in the solid-state, thin films were prepared using pre-cleaned glass slides as the substrate. Zn(II) complexes were dissolved in HPLC-grade CHCl $_3$ to make 1 mg/mL solutions which were passed through a 0.22 μ m PTFE filter and spun-coat using a Laurell Spin Coater WS-650 at 2000 rpm for 30 s. Annealed films were heat-treated on a hot plate at 125 °C for 15 min. Fluorescence spectra were obtained using Cary Eclipse fluorescence spectrophotometer using a quartz cuvette; care was taken to make sure that the solutions did not exceed absorbance values above 0.2 to minimize the inner filter effect.

Electrochemical data were obtained using an Autolab PGSTAT 302 N Exo Chemie potentiostat. Cyclic voltammetry (CV) was carried out in an electrolyte solution of 0.1 M Bu₄NPF₆ in extra dry dichloromethane (DCM, Acros Organics) with ferrocene/ferrocenium as the internal standard. The solution was purged with DCM saturated N₂ for 15 min. A glassy carbon electrode which served as the working electrode, and a platinum electrode which served as the quasi-reference were freshly polished prior to each measurement. A platinum wire served as the counter electrode. Solutions of approximately 5 mg of materials were fully dissolved in the electrolyte solution before each measurement. Measurements were performed with a scan rate of 0.1 V/s. The highest-occupied molecular orbital (HOMO) and lowest-unoccupied molecular orbital (LUMO) energy levels were estimated from the onset of oxidation and reduction potentials, respectively, using the equations:

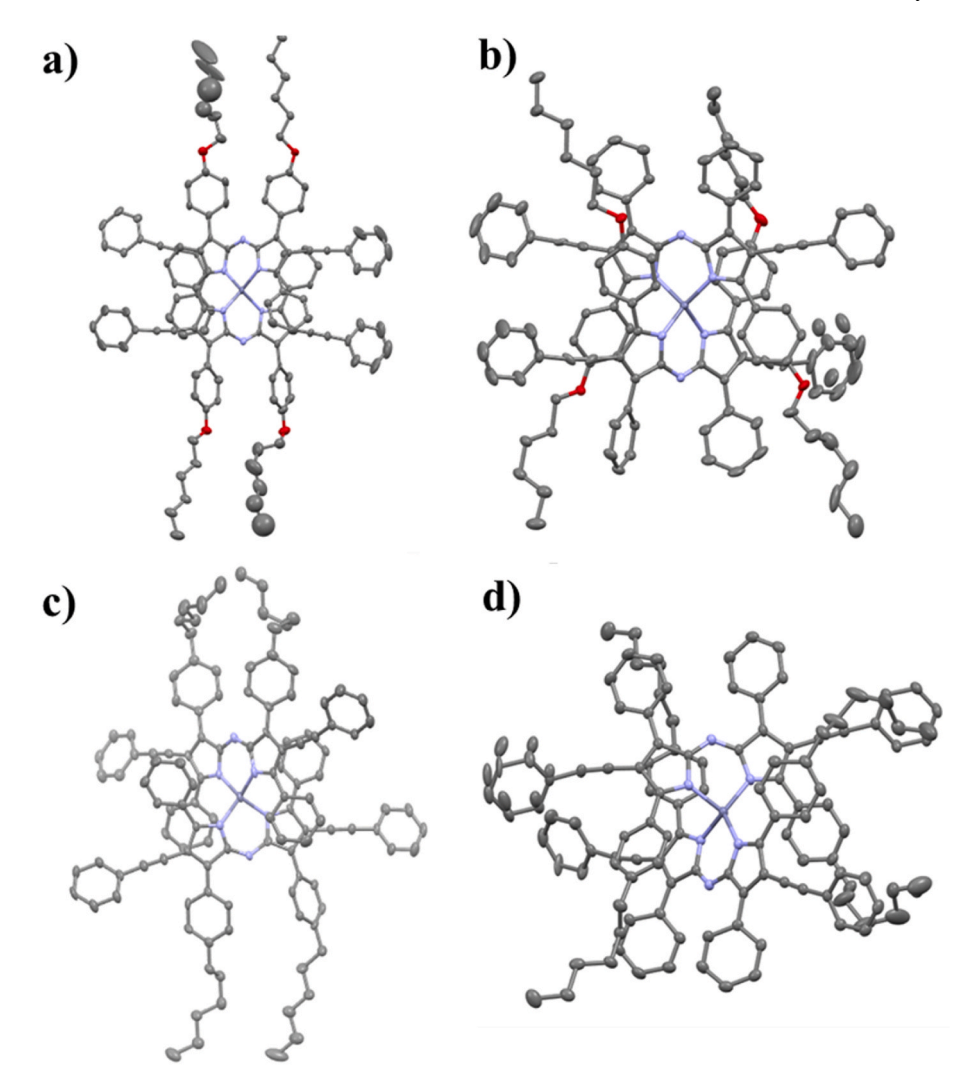


Fig. 2. Ellipsoid plots with 50% probably for: a) Zn(dOhexWS3)₂, b) Zn(pOhexWS3)₂, c) Zn(dhexWS3)₂, d) Zn(phexWS3)₂. Note that for a) and b), one of two structural isomers (different arrangement of solubilizing groups) is shown; c) and d) only have one structural isomer.

$$HOMO = -(E_{onset,ox,vs\ Fc/Fc+} + 4.8\ eV)$$

$$LUMO = -\left(E_{onset,red,vs\ Fc/Fc+} + 4.8\ eV\right)$$

Thermogravimetric analysis (TGA) was performed on a TA instrument Q500 thermogravimetric analyzer using platinum pans. The sample was heated at a ramp rate of 10 °C/min under $\rm N_2$ flow. Differential scanning calorimetry was performed on a TA instrument Q2000 differential scanning calorimeter with a ramp rate of 10 °C/min from 50 to 350 °C under two heat/cool cycles using hermetically sealed aluminum pans (TA Instruments). Samples were recrystallized then dried under vacuum at 90 °C overnight prior to thermal measurements.

Suitable crystals were grown from THF:pentanes via vapor diffusion. Single-crystal X-ray diffraction studies were carried out using a Bruker Microstar diffractometer using Cu Ka ($\lambda=1.54178\ \mbox{\sc A}$) radiation monochromated using laterally graded multilayer (Goebel) mirror focusing optics. A single crystal was mounted on a nylon loop and cooled to 100 K for data collection. Unit-cell parameters were measured and data were collected using the Bruker Apex III software. Data were re-indexed and integrated using the S4 Bruker software, scaled, and corrected for absorption using SAINT. The space groups were assigned and the structures solved by direct methods using the SHELXTL suite of programs and refined by full matrix least squares against F2 with all reflections using Shelxl 2014 and graphical interface Shelxle.2 H atoms attached to carbon atoms were positioned geometrically and constrained to ride on

their parent atoms, with carbon hydrogen bond distances of 0.95 Å for aromatic C–H and 0.99 Å for alkane moieties, respectively. Uiso(H) values were set to 1.2 times Ueq(C). In some cases, there are structural isomers within the unit cell and we report the thermoellipsoid plots on one isomer. Some hexyl-chains were left isotropic due to the chains being highly disordered but nonetheless provides an unambiguous representation of the proposed crystal structure.

Polarized light microscopy (PLM) was carried out on an Olympus BX60f on the annealed films. Samples were prepared from a 1 mg/mL solution of CHCl $_3$ spun-coated onto cleaned glass slides, then annealed similarly with the UV–Vis samples.

3. Results and discussion

3.1. Synthesis

Synthesis of the complexes generally followed previously published synthesis methods and is summarized in Scheme 1 [9,14,24]. Zn(II) complexes with solubilizing groups on the distal phenyls are obtained from *para*-substituted benzaldehyde precursors (1) whereas Zn(II) complexes with solubilizing groups on the proximal phenyls are obtained from *para*-substituted acetophenone precursors (2). The precursor with the hexyl substitution 1b and 2b were synthesized according to the literature [9,14]. The precursors with hexyloxy substitutions were obtained using the Williamson ether reaction of 1-bromohexane with

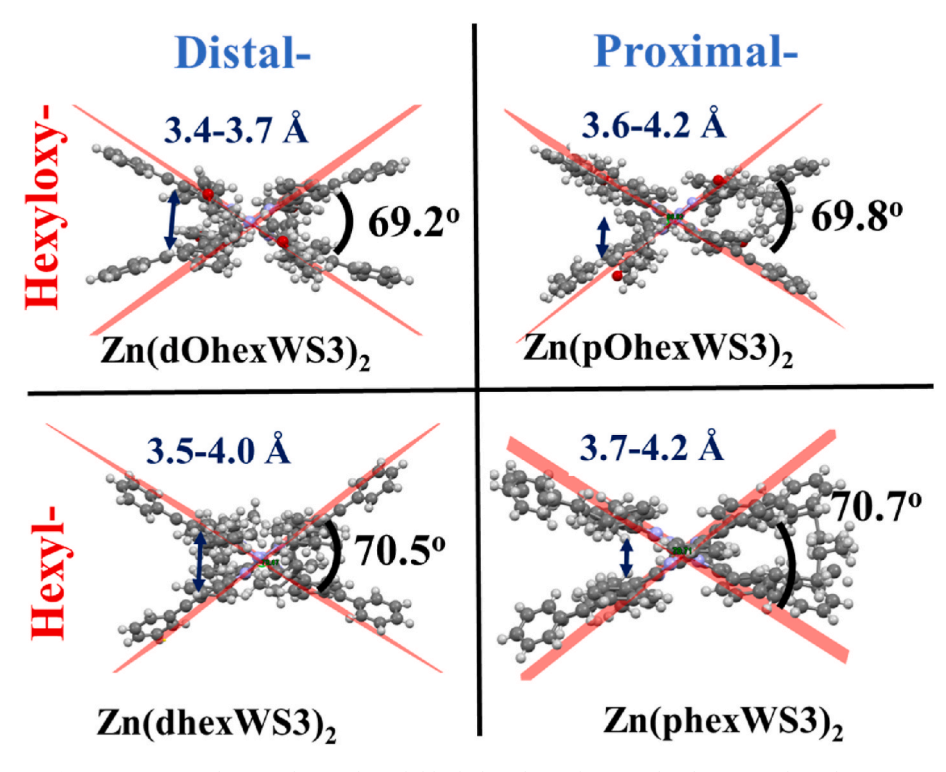


Fig. 3. Zn(II) complexes with intra-ligand dihedral angles and intramolecular π - π stacking distances.

para-hydroxy benzaldehyde or para-hydroxy acetophenone to give 1c and 2c, respectively. All precursors were purified via short-path distillation resulting in isolable yields between 60 and 85%. The appropriate precursors were used to form chalcones by Michael addition, followed by condensation to give free ligands (4). The ADP ligands were then iodinated using N-succinimide to facilitate addition of phenylethynyl groups via Stille coupling (5). Zinc(II) complexation was achieved by deprotonation of 5 using NaH followed by reaction with zinc acetate. The details for the synthesis and characterization of Zn(phexWS3)₂ (6d) can be found in our previous publication [14]. All other zinc complexes (6) were purified by column chromatography followed by slow recrystallization using either THF:MeOH solvent diffusion or THF:pentane vapor diffusion methods. Their identity and purity were confirmed by ¹H NMR, ¹³C NMR, MALDI-TOF MS and elemental analysis.

3.2. Crystal structure

The ellipsoid plots of the complexes are shown in Fig. 2. The complexes have the typical distorted tetrahedral geometry for M(II) homoleptic complexes of ADP [10,25,26]. The solubilizing groups that are placed on the distal phenyls (Fig. 2a and c) extend away from the conjugated core, whereas the solubilizing groups on the proximal phenyls (Fig. 2b and d) overlap with the distal phenyls of the other ligand. Fig. 3 illustrates the dihedral angle between the planes of the ligands with the Zn(II) in the complexes along with the intramolecular $\pi\text{-}\pi$ interactions

between the proximal phenyls of one ligand to the pyrrole group on the ADP-core of the other ligand. For the complexes with hexyloxy solubilizing groups, the dihedral angle is very similar for both distal and proximal placements, at 69.2° and 69.8° , respectively. On the other hand, the angle is relatively bigger with hexyl groups. The dihedral angle of the proximal hexyl group is 70.7° , as reported in literature, whereas the proximal placement has a dihedral angle of 70.5° . The dihedral angle is expected to affect the intramolecular π - π distances between the pyrrole of one ligand and proximal phenyl of the other ligand. Analysis of the intramolecular π - π stacking distance yielded mixed results. The intramolecular π - π stacking found in $Zn(dOhexWS3)_2$ (shown in Fig. 3) was indeed the smallest, at 3.4–3.7 Å, followed by both proximal-substituted complexes with distances of 3.6–4.2 Å.

Because of the difference in the intra-ligand and π - π stacking values between each complex, we measured the key bond angles and distances (Table 1) to see how the solubilizing groups affect the distorted tetra-hedral geometry. All of the complexes have aza-bond (C–N–C) angles within 127°, the N–Zn(II)–N bond angle coming from the chelation within 93–96° and the Zn(II)–N bond distances of ~2.0 Å. Between two chromophores, we observed that the bond angle of the N–Zn(II)–N has a smaller range in the distal-modified complexes of around 105–109°, whereas the proximal-modified complexes ranges from 105 to 111° for Zn(pOhexWS3)₂ and 97–121° for Zn(phexWS3)₂. These observations suggest that the placement of the solubilizing groups on the proximal position influences the bond angle between the two chromophores; the

Table 1
Summary of aza-bond angles (C-N-C), of N-Zn(II)-N for both chelate and between the two chromophores and the bond distance of Zn(II)-N for each complex.

Compound	Bond angles (°)	Bond angles (°)			
	C-N-C	N-Zn(II)-N ^a	N–Zn(II)–N ^b	Zn(II)–N	
Zn(dOhexWS3) ₂	126.93-128.59	93.68-95.28	105.14–108.97	1.957-2.002	
Zn(dhexWS3) ₂	126.46-128.48	93.85-96.16	105.62-108.68	1.959-1.996	
Zn(pOhexWS3) ₂	126.13-128.31	93.72-96.05	104.77-110.76	1.984-1.992	
Zn(phexWS3) ₂	127.40	95.24	96.72-121.39	1.978-1.999	

a N-Zn(II)-N angle of the ADP-Zn(II) interaction.

^b N-Zn(II)-N angle between the two ADP units.

Table 2 Summary of thermal properties.

Compound	T _{d5} (°C)	T _{m1} (°C)	T _{m2} (°C)	T _c (°C)
Zn(WS3) ₂	517 ^a	_	_	340
Zn(dOhexWS3)2	419	240	245	_
$Zn(dhexWS3)_2$	375	147	202	-
$Zn(pOhexWS3)_2$	413	202	_	301
Zn(phexWS3) ₂ ^b	454	210	_	120

^a Zn(WS3)₂ values from the literature [24].

^b Zn(phexWS3)₂ values previously reported as Zn(L1)₂ [14].

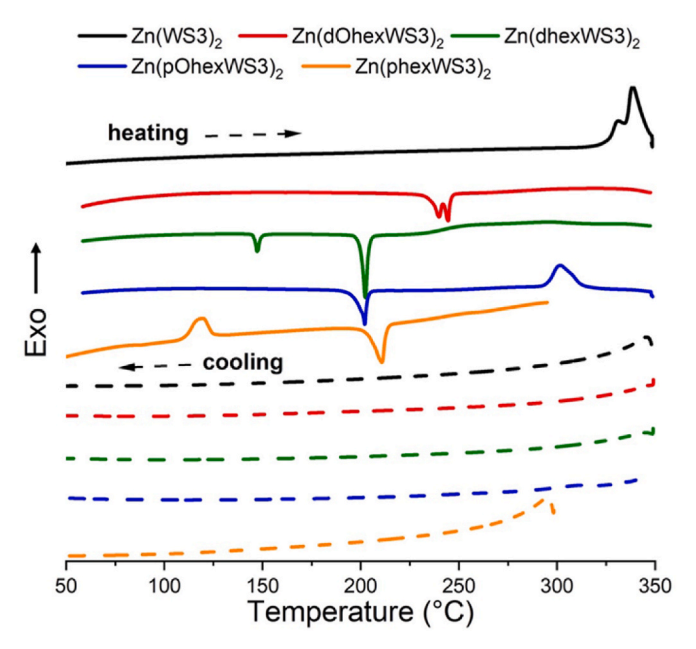


Fig. 4. DSC thermograms showing the 1st heating and cooling cycle.

hexyl group exacerbates the distortion and the hexyloxy group stabilizes the structural geometry. This effect is not observed when the solubilizing groups are placed on the distal phenyl positions.

3.3. Thermal properties

Thermal gravimetric analysis (TGA) showed that all complexes are thermally stable, with decomposition temperatures at 5% weight loss (Td5) ranging from 375 to 517 °C, see Fig. S20 and Table 2. The unsubstituted Zn(WS3) $_2$ has the highest Td5 at 517 °C, and the presence of the hexyl or hexyloxy groups lowers the Td5.

The Zn(II) complexes were further characterized by differential scanning calorimetry (DSC). Fig. 4 shows the DSC 1st heating and cooling cycles; the 2nd heating and cooling cycles are not shown because they are featureless, consistent with the complexes forming an amorphous solid upon cooling at 10 °C/min [14]. Zn(WS3)2 only shows an exothermic crystallization peak around 340 °C during the heating phase. The absence of a melting temperature suggests that the recrystallized Zn (WS3)₂ is amorphous, which is consistent with the fact that we have not been able to get crystals of Zn(WS3)₂ suitable for XRD. All complexes that contain alkyl or alkoxy groups have melting temperatures, suggesting that the side-chains facilitate crystallization; all four crystals were suitable for XRD, as discussed in the previous section. The complexes that have solubilizing groups on the distal phenyls show two endothermic peaks. The first peak (at lower temperature) has a relatively small area compared to the second peak and is attributed to 'melting' of the solubilizing groups (T_{m1} in Table 2). The second peak is attributed to melting of the complex (T_{m2}). The melting temperatures are 240 °C and 245 °C for Zn(dOhexWS3)2, and 147 °C and 202 °C for Zn

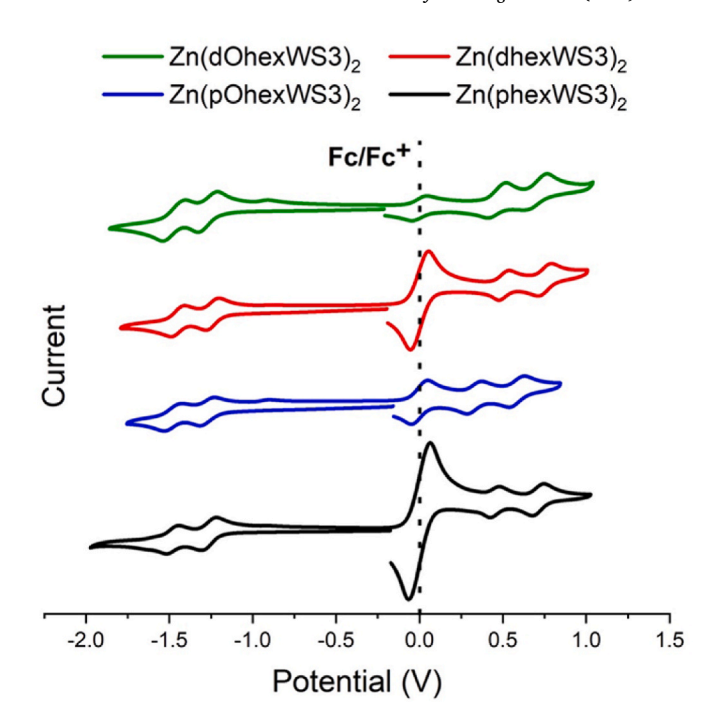


Fig. 5. Cyclic voltammogram of the Zn(II) complexes in solution with Fc/Fc⁺ as the internal standard.

(dhexWS3)₂, respectively. The higher temperatures observed for Zn (dOhexWS3)₂ suggests that the hexyloxy groups on the distal phenyls improve the tendency to crystallize more than the hexyl groups. On the other hand, the complexes with solubilizing groups on the proximal phenyls showed one melting (endothermic) and one crystallization (exothermic) peak. The melting temperatures for Zn(pOhexWS3)₂ and Zn(phexWS3)₂ are similar, at 202 °C and 210 °C, respectively, suggesting the nature of the solubilizing group does not affect the melting point when placed on the proximal phenyls. On the other hand, the crystallization temperatures for Zn(pOhexWS3)₂ and Zn(phexWS3)₂ are very different at 301 °C and 120 °C, respectively. The crystallization is thus strongly influenced by the nature of the solubilizing group.

3.4. Electrochemical properties

The cyclic voltammograms of all complexes in solution are shown in Fig. 5 and the electrochemical properties are summarized in Table 3. Data from the previously published Zn(phexWS3)₂ and Zn(WS3)₂ are included for comparison. All Zn(II) complexes exhibit two reversible oxidation and two reversible reduction processes in solution, typical for these types of complexes [14,24,26]. The reduction potentials ($E_{1/2\text{red}}$) of all of the complexes are similar (within 0.03 V) and thus not affected by the solubilizing groups. The first oxidation potential $(E_{1/2ox})$ of Zn (dOhexWS3)2 and Zn(dhexWS3)2 are similar to that of Zn(WS3)2, while the second oxidation potential of Zn(dOhexWS3)2 is 0.08 V lower than Zn(WS3)2. The first and second oxidation potentials were more greatly affected by solubilizing groups on the proximal phenyls: the oxidation potentials for Zn(phexWS3)2 were 0.05 and 0.06 V lower than Zn (WS3)3, respectively, while those for Zn(pOhexWS3)2 are 0.17 V and 0.19 V lower than Zn(WS3)₂. The greater effect of the hexyloxy groups on oxidation potentials than the hexyl groups is due to the stronger electron donating strength of hexyloxy groups.

The HOMO and LUMO energy levels were estimated from the onsets of the first oxidation and first reduction waves, respectively, and their levels trend with their electrochemical properties. The LUMO energy levels of all complexes are similar at -3.6 eV. The HOMO energy levels for all of the complexes are similar except for $\text{Zn}(\text{pOhexWS3})_2$, which increases to nearly -5 eV. As a result, $\text{Zn}(\text{pOhexWS3})_2$ has the smallest

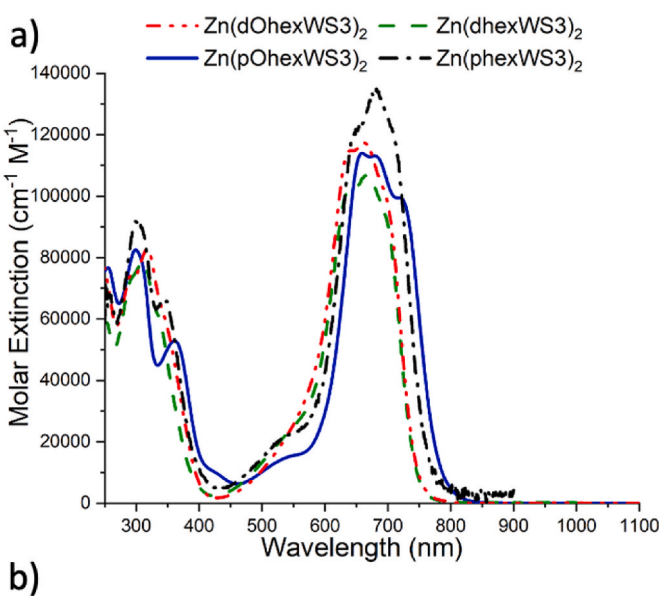
 Table 3

 Summary of the electrochemical properties of the Zn(II) complexes.

	E _{1/2 ox}	$E_{(p,a)}$	E _{1/2 red}	E _(p,c)	E _{ox} onset	НОМО	E _{red} onset	LUMO	$E_{g,elec}$
	V	v	v	V	V	eV	v	eV	eV
Zn(WS3) ₂ ^a	0.50, 0.77	0.58, 0.86	-1.25, -1.47	-1.33, -1.55	0.42	-5.22	-1.14	-3.66	1.62
Zn(dOhexWS3)2	0.47, 0.69	0.52, 0.77	-1.27, -1.47	-1.33, -1.54	0.38	-5.18	-1.21	-3.59	1.59
$Zn(dhexWS3)_2$	0.51, 0.75	0.54, 0.79	-1.24, -1.45	-1.28, -1.49	0.44	-5.24	-1.18	-3.62	1.62
Zn(pOhexWS3) ₂	0.33, 0.58	0.38, 0.63	-1.28, -1.48	-1.32, -1.53	0.27	-5.07	-1.20	-3.60	1.47
Zn(phexWS3) ₂ ^b	0.45, 0.71	0.48, 0.75	-1.27, -1.49	-1.31, -1.52	0.39	-5.19	-1.20	-3.60	1.59

a From ref. [24].

^b From ref. [15].



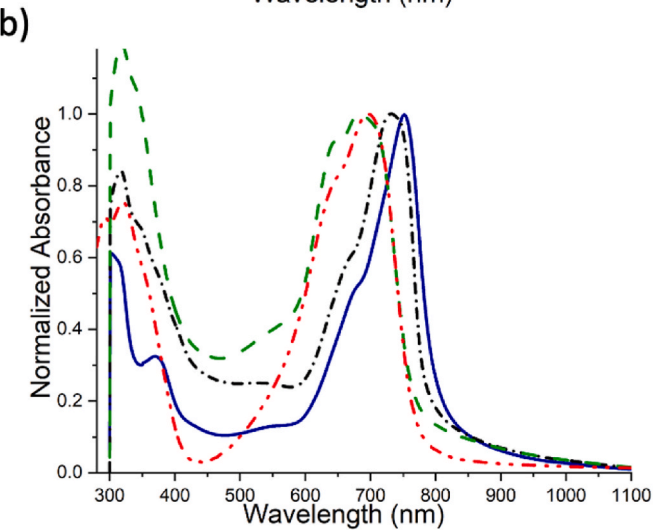


Fig. 6. UV–Vis spectra of complexes a) in $CHCl_3$ solutions, b) films cast from $CHCl_3$ solutions.

electrochemical gap (E_g) at 1.47 eV, compared to around 1.60 eV for the other complexes. These findings are consistent with the optical gaps reported in the previous section.

3.5. Optical properties

The optical properties in solution are shown in Fig. 6 and summarized in Table 4. Data for Zn(WS3)₂ was included in Table 4 for comparison. The solution spectra were typical for this type of complexes: they strongly absorb between 600 and 800 nm with molar absorption

coefficients greater than 100,000 cm $^{-1}$ M $^{-1}$. The $\lambda_{\rm max}$ for the complexes with distal substitutions are similar (663 nm and 667 nm for hexyloxy and hexyl, respectively) and slightly blue-shifted from that of Zn(WS3)₂ (674 nm). On the other hand, the $\lambda_{\rm max}$ for the complexes with substitutions on the proximal phenyls are significantly different (722 nm and 680 nm for hexyloxy and hexyl, respectively) and are red-shift compared to Zn(WS3)₂ (674 nm). This is consistent with previous studies that show that electron donating groups have a stronger effect on optical properties when installed on the proximal phenyls rather than the distal phenyls [1]. The Zn(II) complexes did not show any detectable emission, which is typical for homoleptic metal(II) complexes of aza-dipyrromethene [25,26].

To investigate the optical properties in film, chloroform solutions were spun-coated onto clean glass slides and the optical properties were evaluated for as-cast and annealed films. The optical properties for the as-cast films are shown in Fig. 6b and summarized in Table 4. The Zn (pOhexWS3)2 film appeared slightly blue-green in color whereas the other complexes' films were a darker blue color. The optical gaps were estimated from the absorption onsets. For the distal phenyl substituted complexes, the optical gap was similar to Zn(WS3)2, at 1.60 eV. For the proximal phenyls, the optical gap was lower, 1.52–1.54 eV. The main absorption band in the visible to NIR region red-shifted upon film formation, consistent with some intermolecular interactions in films. The redshift of the lowest energy peak is reported as RS in Table 4 and varied from 17 nm for Zn(dhexWS3)2-69 nm for Zn(pOhexWS3)2. The redshift is greater for proximal substitutions than distal or no substitutions, and greater for hexyloxy than hexyl groups or no substitution. Films were annealed by placing the glass slide on a hot plate at 125 °C for 15 min. Fig. 7 compares the UV-vis spectra of as-cast with annealed films. Interestingly, the main absorption band for the hexyloxy-substituted complexes broadens upon annealing, with the appearance of absorption at longer wavelengths, whereas the main absorption band of the hexyl-substituted complexes did not change significantly. Annealed films of Zn(WS3)2 also do not show any broadening [13], indicating that this broadening is unique to the complexes with hexyloxy substitution. The hexyloxy substituents thus appear to promote aggregation in films upon annealing.

3.6. Microscopic images

The annealed films of the hexyloxy substituted complexes visually look like the complexes are aggregated, and had an unusual appearance, shown in Fig. 8A for Zn(dOhexWS3)₂ and 8E for Zn(pOhexWS3)₂. Intrigued by these visual appearances, we examined the annealed films under a polarized light microscope (PLM). Images obtained at various magnifications are shown in Fig. 8B-D for Zn(dOhexWS3)₂ and F-H Zn (pOhexWS3)₂. Zn(dOhexWS3)₂ shows feather-like crystals. At 10x magnification, we observe dendritic formation and at 40x magnification and upon further magnification, formations are branching and appear to be interlinked. On the other hand, Zn(pOhexWS3)₂ appears as a hazy film on glass, but upon 4x magnification, we see small crystallites homogeneously dispersed on the surface of the film. At higher magnifications, the crystallites appear as discrete needles. No observable

Table 4
Summary of optical properties of Zn(II) complexes in solution and film.

Compound	Solution		Film as-cast (annealed)			
	$\lambda_{\rm max}$ (nm) ($\varepsilon \times 10^4$ L mol ⁻¹ cm ⁻¹)	λ _{onset} (nm)	λ _{max} (nm)	RS ^a (nm)	λ _{onset} (nm)	E _{opt} (eV)
Zn(WS3) ₂	309 (3.9), 674 (10.5)	757	696	+22	785	1.58
Zn(dOhexWS3)2	289 (7.49), 317 (8.34), 639 (11.5), 663 (11.8)	750	695 (695)	+32 (+32)	775 (819)	1.60 (1.51)
$Zn(dhexWS3)_2$	311 (7.86), 334 (6.12), 636 (10.2), 667 (10.7)	750	684 (696)	+17 (+29)	775 (788)	1.60 (1.57)
Zn(pOhexWS3) ₂	299 (8.26), 360 (5.35), 658 (11.4), 683 (11.3), 722 (9.99)	784	752 (749)	+69 (+66)	815 (889)	1.52 (1.39)
Zn(phexWS3) ₂	300 (9.22), 345 (6.71), 645 (12.1), 680 (13.5)	768	725 (730)	+45 (+50)	802 (825)	1.54 (1.50)

^{**}data for Zn(WS3)₂ is from Ref. [24] and data for Zn(phexWS3)₂ is from reference [15].

^a Redshift of the lowest absorption peak upon film formation.

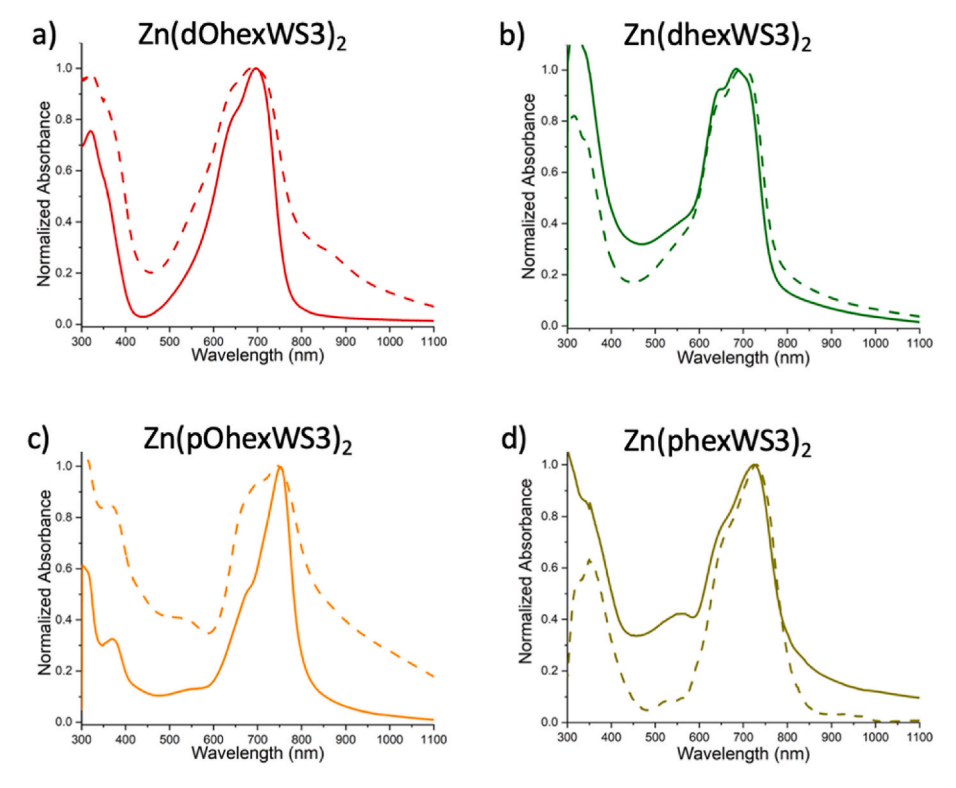


Fig. 7. UV-Vis spectra of as-cast (full line) and annealed (dashed line) films of a) Zn(dOhexWS3)2, b) Zn(dhexhexWS3)2, c) Zn(pOhexWS3)2, d) Zn(phexWS3)2.

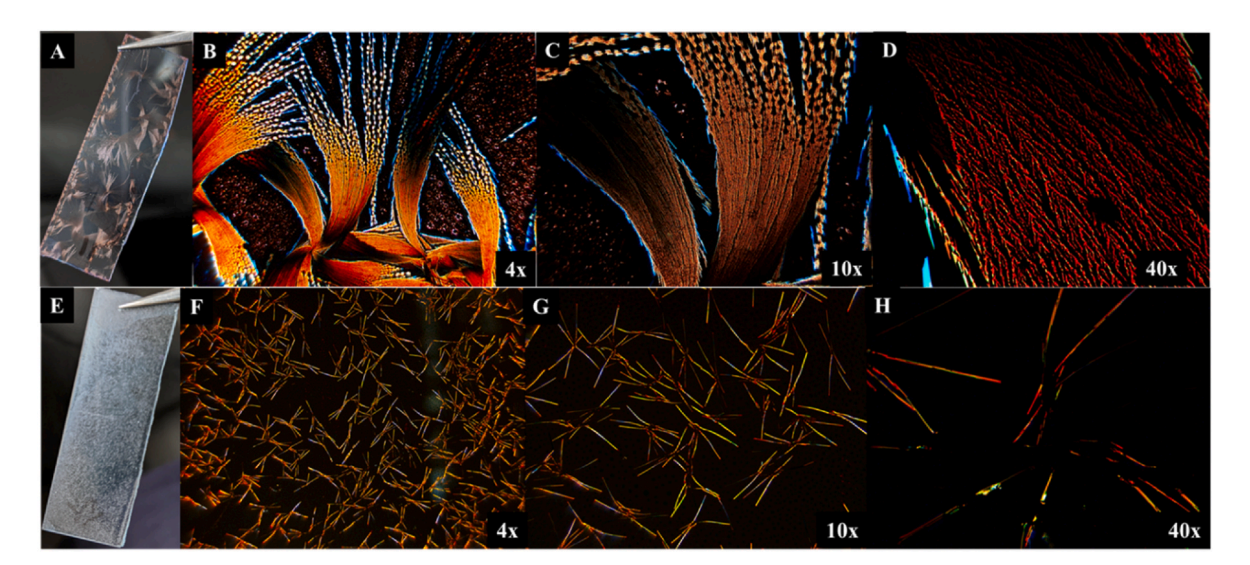


Fig. 8. PLM images of Zn(dOhexWS3)₂ A) annealed film on glass, and microscope images at B) 4x, C) 10x, D) 40x; Zn(pOhexWS3)₂ E) annealed film on glass, and microscope images at F) 4x, G) 10x, H) 40x.

features were seen for the complexes that contain hexyl groups. Placement of the hexyloxy-solubilizing group appears to favor crystallization and self-assembly upon annealing in films. The larger, more ordered crystallite formation in $\text{Zn}(\text{dOhexWS3})_2$ explain the absorption broadening observed upon annealing. Greater order in the solid state is not only advantageous for broadening absorption, but also may result in better charge transport, which is beneficial for electronic devices such as organic photovoltaics, transistors and photodetectors.

4. Conclusions

Zinc(II) complexes of ADP with solubilizing groups (hexyl or hexyloxy) either on the distal or the proximal phenyls were successfully synthesized and characterized. The crystal structure of the functionalized complexes showed the typical distorted tetrahedral geometry for these types of homoleptic complexes. The solubilizing groups on the distal phenyls extend away from the conjugated core and can thus interact with each other whereas the solubilizing groups on the proximal phenyls overlap with the distal phenyls of the other ligand. This placement strongly impacts the transitions observed by DSC: When placed on distal phenyls, two endothermic peaks are observed, the smaller one probably resulting from 'melting' of the solubilizing groups. The melting temperatures are higher for hexyloxy than hexyl, pointing to greater tendency to crystallize with hexyloxy groups. When placed on proximal phenyls, one exothermic (crystallization) peak and one endothermic (melting) peak are observed with no solubilizing group 'melting'. The crystallization peak is much higher for hexyloxy than hexyl. Consistent with previous studies, the electron rich solubilizing groups affect electrochemical and optical properties when placed on the proximal phenyls. They lower the oxidation potential without greatly affecting reduction potentials, red-shift the complex's main absorption band, and lower the optical gap, with the largest effect observed with hexyloxy. As a result, the optical gap is 1.60 eV for the distal-substituted complexes, 1.54 eV for Zn(phexWS3)2 and 1.52 eV for Zn(pOhexWS3)2. Interestingly, the hexyloxy groups were found to drive self-assembly and crystallization much better than hexyls, and their effect is greater when placed on distal phenyls than proximal phenyls. Further studies are required to determine if the order driven by hexyloxy groups enhances charge transport and performance in devices such as organic solar cells, transistors or photodetectors.

CRediT authorship contribution statement

Jayvic C. Jimenez: Performed synthesis and characterization of all complexes, Formal analysis, Manuscript writing. Quynh Tran: Responsible for synthesis and characterization of some complexes, Formal analysis, Manuscript writing. Madison H. Pugh: Contributed to synthesis of complexes. Christina D. Brancel: Contributed to synthesis of complexes. Arnold L. Rheingold: Responsible for the crystal structures. Geneviève Sauvé: Responsible for conception, Project management, Formal analysis, Writing of manuscript.

Declaration of competing interest

The authors declare that they have no known competing financial interests or personal relationships that could have appeared to influence the work reported in this paper.

Data availability

Data will be made available on request.

Acknowledgements

We are grateful to the National Science Foundation (CHEM 19048678) for funding this project, NSF MRI-0821515 for the MALDI-

TOF/TOF and NSF MRI-1334048 for NMR instrumentation. We also thank Dr. John D. Protasiewicz for access to his cyclic voltammetry instrumentation and Dr. Lei Zhu for access to his PLM instrumentation.

Appendix A. Supplementary data

Supplementary data to this article can be found online at https://doi.org/10.1016/j.dyepig.2022.110858.

References

- Loudet A, Burgess K. BODIPY dyes and their derivatives: syntheses and spectroscopic properties. Chem Rev 2007;107:4891–932.
- [2] Palma A, Gallagher JF, Mueller-Bunz H, Wolowska J, McInnes EJL, O'Shea DF. Co (II), Ni(II), Cu(II) and Zn(II) complexes of tetraphenylazadipyrromethene. Dalton Trans 2009:273–9.
- [3] Partyka D, Gao L, Teets T, Updegraff J, Deligonul N, Gray T. Copper-catalyzed huisgen [3 + 2] cycloaddition of gold(I) alkynyls with benzyl azide. Syntheses, structures, and optical properties. Organometallics 2009;28:6171–82.
- [4] Ge Y, O'Shea DF. Azadipyrromethenes: from traditional dye chemistry to leading edge applications. Chem Soc Rev 2016;45:3846–64.
- [5] Killoran J, Allen L, Gallagher JF, Gallagher WM, O'Shea DF. Synthesis of Bf2 chelates of tetraarylazadipyrromethenes and evidence for their photodynamic therapeutic behaviour. Chem Commun 2002:1862–3.
- [6] Loudet A, Bandichhor R, Burgess K, Palma A, McDonnell SO, Hall MJ, O'Shea DF. B,O-Chelated azadipyrromethenes as near-IR probes. Org Lett 2008;10:4771–4.
- [7] Mueller T, Gresser R, Leo K, Riede M. Organic solar cells based on a novel infrared absorbing aza-bodipy dye. Sol Energy Mater Sol Cells 2012;99:176–81.
- [8] Maar RR, Gilroy JB. Group 13 complexes of chelating N₂ O₂(N-) ligands as hybrid molecular materials. Chem Eur J 2018;24:12449–57.
- [9] Jimenez JC, Zhou Z, Rheingold AL, Parker SM, Sauve G. Tuning the properties of azadipyrromethene-based near-infrared dyes using intramolecular BO chelation and peripheral substitutions. Inorg Chem 2021;60:13320–31.
- [10] Mao Z, Senevirathna W, Liao JY, Gu J, Kesava SV, Guo C, Gomez ED, Sauvé G. Azadipyrromethene-based Zn(II) complexes as nonplanar conjugated electron acceptors for organic photovoltaics. Adv Mater 2014;26:6290-4.
- [11] Sauvé G, Fernando R. Beyond fullerenes: designing alternative molecular electron acceptors for solution-processable bulk heterojunction organic photovoltaics. J Phys Chem Lett 2015;6:3770–80.
- [12] Sauve G. Designing alternative non-fullerene molecular electron acceptors for solution-processable organic photovoltaics. Chem Rec 2019;19:1078–92.
- [13] Pejić S, Thomsen AM, Etheridge FS, Fernando R, Wang C, Sauvé G. Fluorination increases the electron mobility of zinc azadipyrromethene-based electron acceptors and enhances the performance of fullerene-free organic solar cells. J Mater Chem C 2018;6:3990–8.
- [14] Wang C, Wei P, Ngai JHL, Rheingold AL, Gray TG, Li Y, Pentzer E, Li R, Zhu L, Sauvé G. A zinc(Ii) complex of di(Naphthylethynyl)Azadipyrromethene with low synthetic complexity leads to OPV with high Industrial accessibility. J. Mater. Chem. A 2019;7:24614–25.
- [15] Wang C, Zhao M, Rheingold AL, Sauvé G. Structure–property study of homoleptic zinc(II) complexes of di(arylethynyl) azadipyrromethene as nonfullerene acceptors for organic photovoltaics: effect of the aryl group. J Phys Chem C 2020;124: 8541–9.
- [16] Zhou Y, et al. High performance all-polymer solar cell via polymer side-chain engineering. Adv Mater 2014;26:3767–72.
- [17] Lin Y, Zhan X. Non-fullerene acceptors for organic photovoltaics: an emerging horizon. Mater Horiz 2014;1:470–88.
- [18] Yurt S, Benanti TL, Venkataraman H, Bheemaraju A, Venkataraman D. Strategies for nanoscale semiconductor assemblies through side chain interactions. Polym Preprint 2010;51:245.
- [19] Cui C, Wong WY. Effects of alkylthio and alkoxy side chains in polymer donor materials for organic solar cells. Macromol Rapid Commun 2016;37:287–302.
- [20] Zhu J, Xiao Y, Wang J, Liu K, Jiang H, Lin Y, Lu X, Zhan X. Alkoxy-induced near-infrared sensitive electron acceptor for high-performance organic solar cells. Chem Mater 2018;30:4150–6.
- [21] Zhu D, Zhu Q, Gu C, Ouyang D, Qiu M, Bao X, Yang R. Alkoxyl side chain substituted thieno[3,4-C]Pyrrole-4,6-Dione to enhance photovoltaic performance with low steric hindrance and high dipole moment. Macromolecules 2016;49: 5788–95.
- [22] Kraner S, et al. Influence of side groups on the performance of infrared absorbing aza-bodipy organic solar cells. Phys. Status Solidi A 2015;212:2747–53.
- [23] Du Z, Chen W, Qiu M, Chen Y, Wang N, Wang T, Sun M, Yu D, Yang R. Utilizing alkoxyphenyl substituents for side-chain engineering of efficient benzo[1,2-B:4,5-B']Dithiophene-Based small molecule organic solar cells. Phys Chem Chem Phys 2015;17:17391-8.

- [24] Senevirathna W, Liao J-y, Mao Z, Gu J, Porter M, Wang C, Fernando R, Sauvé G.
- Synthesis, characterization and photovoltaic properties of azadipyrromethene-based acceptors: effect of pyrrolic substituents. J. Mater. Chem. A 2015;3:4203–14.
 Teets TS, Partyka DV, Updegraff JB, Gray TG. Homoleptic, four-coordinate azadipyrromethene complexes of D(10) zinc and mercury. Inorg Chem 2008;47: 2338-46.
- [26] Senevirathna W, Sauve G. Introducing 3D conjugated acceptors with Intense red absorption: homoleptic metal(II) complexes of di(phenylacetylene) azadipyrromethene. J Mater Chem C 2013;1:6684–94.